Structural, Electronic, Thermodynamic and Nonlinear Optical Properties of a Novel Ce(III) Complex with Ferrocenyl Dithiophosphonate

A. Aydin* and B. Dede

Süleyman Demirel University, Faculty of Engineering & Natural Sciences, Department of Chemistry, 32260 Isparta, Türkiye

Received: 29.04.2025 & Accepted: 13.06.2025

Doi: 10.12693/APhysPolA.148.3 *e-mail: ahmetaydin@sdu.edu.tr

In this study, a novel cerium(III) complex featuring a ferrocenyl dithiophosphonate ligand was synthesized and comprehensively characterized using a range of spectroscopic and analytical techniques. The synthetic route involves the esterification of 2,4-diferrocenyl-1,3-dithiadiphosphetane disulfide (ferrocenyl Lawesson's reagent) with isopropyl alcohol, followed by conversion to its ammonium salt and subsequent complexation with $Ce(NO_3)_3 \cdot 6H_2O$ in tetrahydrofuran. The structure of the complex was elucidated using Fourier transform infrared spectroscopy, ^{1}H- and ^{31}P-nuclear magnetic resonance spectroscopy, thermal analysis, and elemental analysis. Spectroscopic results indicated successful coordination of Ce(III) through the dithiophosphonate moieties. Quantum mechanical calculations at the density functional theory/Becke, 3-parameter, Lee–Yang–Parr level provided insight into the geometric, electronic, and thermodynamic properties of the Ce(III) complex. The total density of states and frontier molecular orbital analyses revealed an energy gap of $\Delta E = 9.042$ eV of the singly occupied–lowest unoccupied molecular orbitals, indicating high electronic stability. Theoretical calculations highlighted the significant nonlinear optical properties of a Ce(III) complex, demonstrating its potential for enhanced nonlinear optical performance due to the synergistic effects of the ferrocenyl dithiophosphonate ligand and Ce(III) ion. Additionally, thermodynamic parameters such as zero-point energy, entropy, and heat capacity were calculated, confirming the structural stability and potential functional applications of the synthesized Ce(III) complex in photophysical or catalytic systems.

topics: dithiophosphonate, cerium complex, density functional theory (DFT), quantum mechanical calculation

1. Introduction

Ferrocene-derived compounds constitute an important research area in organometallic chemistry due to their redox-active structures and stable sandwich-type metal–ligand interactions. The Fe(II) center located between the two cyclopentadienyl rings of ferrocene has many chemical and biological applications, especially due to its reversible redox behavior, thermal stability, and susceptibility to biological interactions [1]. On the other hand, dithiophosphonate ligands can form strong coordination complexes, especially with soft transition metals and rare earth elements, due to their soft sulfur donor atoms. The structural variations of these ligands have a direct impact on the solubility, electronic properties, and redox behavior of metal complexes [2]. Dithiophosphonate ligands have garnered significant attention from the scientific community due to their wide-ranging applications in both academic and industrial domains, including their use as lubricant additives, pesticides, and chemical warfare agents. Notably, some of these complexes exhibit antitumor activity and have therefore been investigated in the context of chemotherapy research. While numerous studies have focused on the coordination chemistry of dithiophosphonic acid with transition metals, investigations involving lanthanide complexes remain relatively scarce [3–6].

Complexes of ferrocenyl dithiophosphonate ligands with cerium ions are an area of research that has not yet been sufficiently studied both structurally and electronically. The synthesis and characterization of such complexes, especially using spectroscopic and quantum chemical analysis, can provide new insights at both experimental and theoretical levels. Indeed, the photoluminescence, electrochemical activity, and optoelectronic behaviors observed in complexes formed by similar structures with transition metals show that these systems are promising for advanced materials applications [7].

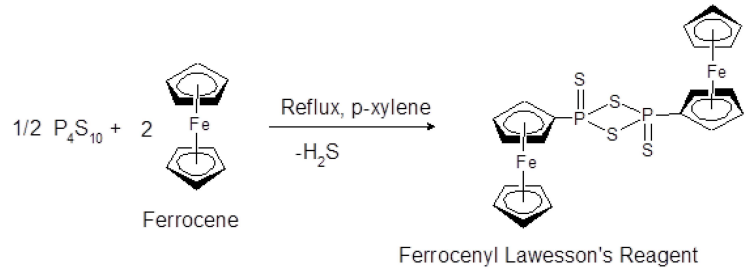

Fig. 1. Synthesis of ferrocenyl Lawesson's reagent.

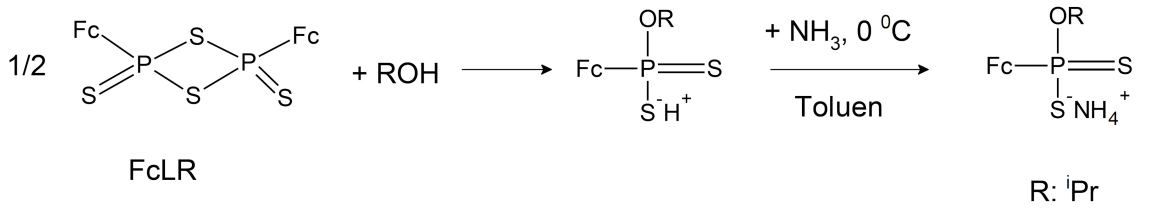

Fig. 2. Synthesis of ammonium ferrocenyl dithiophosphonate.

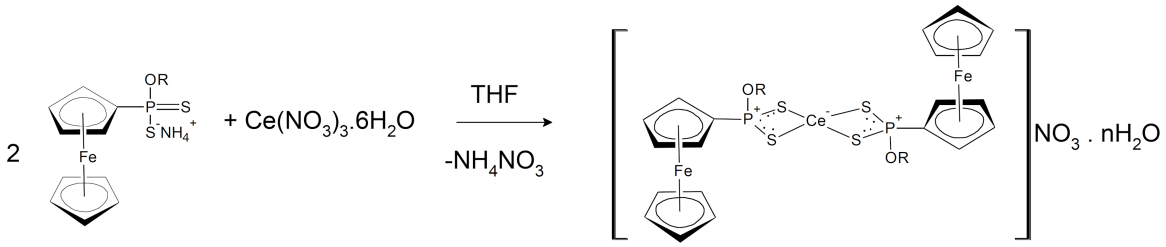

Fig. 3. Synthesis reaction of Ce(III) complex.

In this context, the main aim of our study is to synthesize a new ferrocenyl dithiophosphonate derivative complex with cerium(III) ion, to perform detailed spectroscopic characterizations of these complexes, and to reveal the structure–electronic property relationships by quantum mechanical calculations. Within the scope of this study, 2,4-diferrocenyl-1,3-dithiophosphetane-2,4-disulfide, commonly referred to in the literature as the "ferrocenyl Lawesson's reagent", was synthesized by reacting phosphorus pentasulfide dimer (P_4S_{10}) with a stoichiometric amount of ferrocene [$Fe(C_5H_5)_2$] in an appropriate solvent medium (Fig. 1).

Subsequently, the addition of isopropyl alcohol (^{i}PrOH) to the dimeric structure of the ferrocenyl Lawesson's reagent yielded the ferrocenyl dithiophosphonic acid O-alkyl ester, which was then treated with anhydrous ammonia gas and isolated from the reaction medium in the form of ammonium salt (Fig. 2) [8, 9].

The Ce(III) complex was synthesized by reacting the previously prepared ammonium salt of the ferrocenyl dithiophosphonic acid O-alkyl ester with $Ce(NO_3)_3.6H_2O$ in a tetrahydrofuran (THF) medium. Assuming a four-coordinate geometry, the reaction equation is as illustrated in Fig. 3.

The structure of the synthesized Ce(III) complex was elucidated using elemental analysis, thermal analysis, Fourier transform infrared (FTIR) spectroscopy, and ^{1}H- and ^{31}P-nuclear magnetic resonance (NMR) spectroscopy.

2. Materials and methods

2.1. Physical measurements

The melting point of the molecule was determined without correction using a Gallenkamp apparatus. The elemental analysis was performed with the LECO CHNS-932 instrument. IR (infrared) spectra were recorded on a Mattson 1000 FTIR spectrometer using KBr pellets in the range of 4000–400 cm^{-1}. ^{1}H- and ^{31}P-NMR spectra were acquired in DMSO-d_6 (dimethyl sulfoxide-d_6) on

Bruker DPX 400 FT-NMR spectrometer. Thermal analyses were conducted using a Perkin Elmer Diamond thermogravimetric analyzer.

2.2. Synthesis of [bis-O-isopropyl (ferrocenyl) dithiophosphonate] cerium(III) nitrate tetrahydrate complex

The synthesis of NH_4L was carried out following a method outlined in the literature for analogous compounds [10, 11]. A solution of 0.5 g of ammonium O-isopropyl ferrocenyl dithiophosphonate in 10 mL of tetrahydrofuran (THF) was prepared in a 100 mL flask equipped with a reflux condenser. To this solution, 0.2 g of $Ce(NO_3)_3 \cdot 6H_2O$ dissolved in 10 mL THF was added dropwise in the appropriate stoichiometric ratio. The mixture was heated for 5–10 min, and the NH_4NO_3 byproduct formed during the reaction was removed by filtration. The resulting oily substance was then solidified by the addition of diethyl ether, washed with alcohol, and allowed to crystallize from a dichloromethane–methanol (1:1) mixture. The Ce(III) complex was obtained as a dark green precipitate, which was subsequently washed with diethyl ether and dried under vacuum in a desiccator.

The Ce(III) complex was obtained with a yield of 0.42 g (96%) and a decomposition point of 176°C. In elemental analysis, the calculated (found) values for $CeP_2S_4Fe_2C_{26}H_{40}NO_9$ were C 32.78% (30.13%), H 4.23% (2.99%), and S 13.46% (12.05%). IR spectrum (KBr) showed absorptions at 3368 (υ_{O-H}), 1383 cm^{-1} (υ_{N-O-}), 1179 cm^{-1} (υ_{P-O-C}), 669 cm^{-1} ($\upsilon_{asymP-S}$), 560 cm^{-1} ($\upsilon_{symP=S}$).

2.3. Computational methods

The Gaussian 09 software suite was used to perform quantum chemical calculations of the Ce(III) complex [12]. The GaussView 5.0.9 program was employed for visualizations [13]. The ground state molecular geometry of the Ce(III) complex was optimized at the density functional theory/Becke, 3-parameter, Lee–Yang–Parr (DFT/B3LYP) level using the def2-SVP basis set for the Fe(II) and Ce(III) ions and the 6-311G(d,p) basis set for the other atoms [14–16]. The total density of states (TDOS) plot of the molecule was generated with the GaussSum 3.0 program [17]. The thermodynamic parameters of the Ce(III) complex were obtained using the Shermo software [18]. The output file of the frequency calculation of the molecule performed at the mentioned level was used for this procedure. The molecular dipole moment (μ), mean polarizability ($\tilde{\alpha}$), polarizability anisotropy ($\Delta\alpha$), and first hyperpolarizability (β_{tot}) of the Ce(III) complex were calculated using the finite field (FF) approach as implemented in the Gaussian 09 software package. Single-point calculations were performed on the optimized geometry using the keywords Polar and Field = Read to apply an external electric field of ± 0.001 a.u. in x, y, and z directions. In addition to the B3LYP functional, CAM-B3LYP (CAM — Coulomb-attenuating method), i.e., a long-range corrected functional known for better treatment of intramolecular charge transfer effects, was also employed to evaluate the nonlinear optical properties of the Ce(III) complex. B3LYP and CAM-B3LYP functionals were used, with the def2-SVP basis set for Fe(II) and Ce(III) ions and the 6-311G(d,p) basis set for all remaining atoms.

3. Results and discussion

3.1. Characterization

The Ce(III) complex with the formula $CeP_2S_4Fe_2C_{26}H_{40}NO_9$ was prepared by the reaction of the ammonium salt of ferrocenyl dithiophosphonic acid with the $Ce(NO_3)_3 \cdot 6H_2O$ salt in THF solvent. The IR spectrum of the Ce(III) complex showed O–H stretching vibration due to H_2O at 3368 cm^{-1} and N–O stretching vibration of the nitrate group at 1383 cm^{-1}. The band observed at 1179 cm^{-1} in the spectrum of the Ce(III) complex corresponded to the P–O–C stretching vibration. The characteristic $\upsilon_{asymP-S}$ and $\upsilon_{symP=S}$ stretching vibrations of the molecule appeared at 669 and 560 cm^{-1}, respectively.

The presence of four moles of hydrate water in the Ce(III) complex structure was confirmed by thermal analysis, as illustrated in Fig. 4. The thermal decomposition profile revealed a mass loss at approximately 136°C, which corresponds to the release of four moles of crystallization water. This observed mass loss is consistent with the elemental analysis results and supports the proposed geometric structure of the Ce(III) complex.

No X-ray quality single crystal of the Ce(III) complex was obtained. The ^{1}H-NMR spectrum of phosphorus interaction in the Ce(III) complex recorded in DMSO-d_6 showed that the ligand protons in the complex gave broad signals, which were attributed to the presence of unpaired electrons in the valence shell of the Ce(III) ion, leading to broadening and loss of spectral resolution. The peaks observed at $\delta = 4.42$ and 4.17 ppm were assigned to the protons of the phosphorus-substituted ferrocene ring. Among these, the signal at $\delta = 4.17$ ppm appeared downfield relative to the unsubstituted ferrocene ring protons, which gave a broad signal at $\delta = 4.21$ ppm. The broad signal at $\delta = 4.40$ ppm was attributed to the -OCH protons of the alkyl group, while the broad signal at $\delta = 1.20$ ppm was assigned to the methyl protons adjacent to the -CH group. The proton-free ^{31}P-NMR spectrum of the Ce(III) complex recorded in DMSO-d_6 exhibited

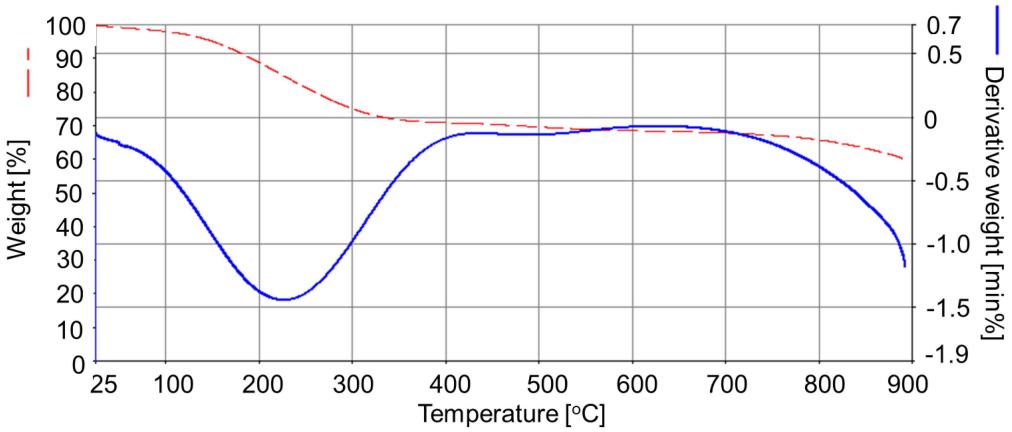

Fig. 4. Thermal analysis diagram of Ce(III) complex.

multiple signals in the range of $\delta = 50$–100 ppm. This multiplicity was a known characteristic of paramagnetic metal complexes and was caused by the unpaired electron on the metal center, which generated local magnetic fields, induced signal splitting, and accelerated relaxation processes, resulting in a broadened spectrum. The data of the synthesized Ce(III) complex were in good agreement with the values of similar compounds in the literature [19–21].

3.2. Quantum mechanical calculations

3.2.1. Optimized molecular geometry

The optimized molecular geometry of the synthesized Ce(III) complex was calculated at the DFT/B3LYP/def2-SVP and DFT/B3LYP/6-311G(d,p) levels of theory for the metal and other atoms, respectively. Figure 5 shows the optimized molecular geometry of the molecule with numbered atoms, and some significant parameters obtained from this geometry, i.e., bond lengths, bond angles, and dihedral angles, are given in Table I. The optimized geometry data of the complex formed by bis-O-isopropyl(ferrocenyl)dithiophosphonate with Ce(III) ion provided detailed information on the ligand's coordination behavior and the complex's three-dimensional structure. The Fe–C bond lengths in the ferrocene moieties (2.312–2.361 Å) indicate a typical η^5-coordinated ferrocene system. These values suggest that the ferrocene unit remains geometrically intact and the interaction with the metal center during complexation takes place via phosphorus and sulfur atoms. The bond lengths between the phosphorus and sulfur atoms of the ligand (2.046 Å in P12-S13, 2.054 Å in P46-S48) were within the typical limits of the dithiophosphonate group, confirming the coordination of the

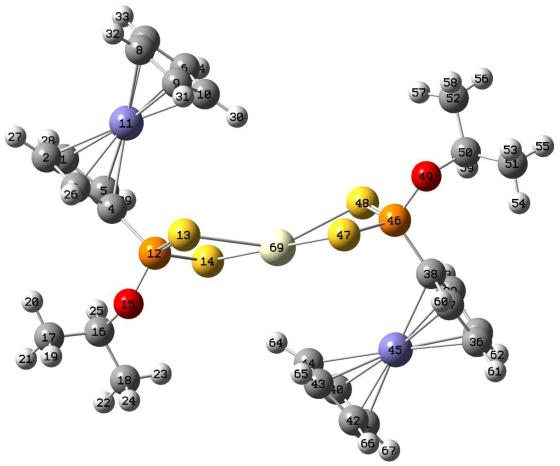

Fig. 5. Optimized molecular geometry of Ce(III) complex with numbered atoms.

ligand with Ce(III) via the soft donor S atoms. The S–Ce bond lengths in the range 2.822–2.879 Å indicate that the soft S donor atoms interacted with Ce(III) with moderate strength.

The C4–P12–S13 and C38–P462–S48 bond angles between the ferrocene and dithiophosphonate units were calculated to be approximately 110°. Similarly, the C4–P12–O15 and C38–P46–O49 bond angles between the ferrocene, dithiophosphonate, and O-isopropyl moieties in the Ce(III) complex were obtained as 109.8° and 110.9°, respectively. The bond angles S47–Ce69–S48 and S13–Ce69–S14 around the Ce(III) ion in the synthesized metal complex, calculated to be 72.6° and 72.2°, respectively, revealed that the Ce(III) complex has a distorted square planar geometry. On the other hand, the dihedral angles of Fe11–C4–P12–O15 and Fe45–C38–P46–O49 were calculated to be 162.5° and 169.7°, respectively, indicating that the ferrocene, dithiophosphonate, and O-isopropyl units in the Ce(III) complex do not lie in the same

TABLE I

Some selected calculated bond lengths [Å] and bond and dihedral angles [°] for Ce(III) complex.

Geometric parameters	Bond lengths [Å]
C8–Fe11	2.312
C4–Fe11	2.361
C38–Fe45	2.326
C42–Fe45	2.326
C4–P12	1.773
C38–P46	1.786
P12–S13	2.046
P46–S48	2.054
P12–O15	1.577
P46–O49	1.568
S13–Ce69	2.822
S14–Ce69	2.876
S47–Ce69	2.879
S48–Ce69	2.839
Geometric parameters	Bond angles [°]
C5–Fe11–C10	126.1
C36-Fe45-C42	116.4
C4–P12–S13	111.0
C38–P462–S48	107.8
S13–P12–S14	111.1
S47–P46–S48	111.1
C4–P12–O15	109.8
C38–P46–O49	110.9
S13–Ce69–S14	72.6
S47–Ce69–S48	72.2
Geometric parameters	Dihedral angles [°]
Fe11–C4–P12–O15	162.5
Fe45–C38–P46–O49	169.7
S13–P12–S14–O15	115.4
S47–P46–S48–O49	119.2

plane. Furthermore, the fact that the dihedral angles S13–P12–S14–O15 and S47–P46–S48–O49 were not equal to or close to 180° or 0° also supports that the dithiophosphonate and O-isopropyl moieties do not lie in the same plane.

3.2.2. Molecular electrostatic potential diagram

A molecular electrostatic potential (MEP) map is a 3D visualization of the electrostatic potential distribution across a molecule's van der Waals surface, providing critical insights into its electron density variations and charge localization. These diagrams are widely employed to analyze chemical systems' reactive sites, intermolecular interactions, and polarity patterns. In MEP diagrams, the red and blue regions correspond to areas of high and low electron

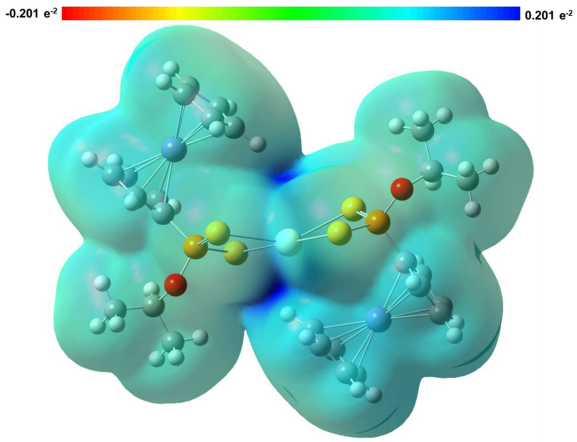

Fig. 6. MEP surface diagram of Ce(III) complex.

density, respectively. Green zones indicate neutral or weakly polarized regions of a molecule. The calculated MEP surface diagram of the synthesized Ce(III) complex is shown in Fig. 6.

In the MEP diagram of the Ce(III) complex, negative potentials were calculated at $-0.201\,e^{-2}$ and positive potentials at $+0.201\,e^{-2}$. In the MEP diagram of the molecule, no region of significant negative or positive electrostatic potential was observed. On the other hand, the presence of little blue regions in the vicinity of the Ce(III) ion indicates the existence of some positive electrostatic potential in this zone. This blue colored area can act as an electrophile in the reactions of the Ce(III) complex with other molecules. Based on the MEP diagram, it was concluded that the electron-withdrawing and donating properties of the ligand are balanced and that there is effective charge-sharing between the Ce(III) center and the ligand. Furthermore, it was determined that the Ce(III)–ligand interaction is predominantly covalent, the charge is delocalized rather than localized, and the complex will not exhibit strong interactions with polar solvents.

3.2.3. Frontier molecular orbitals and total density of states analysis

The total density of states (TDOS) plot and the frontier molecular orbitals (FMOs) shown in Fig. 7 were generated to study in detail the electronic structure of the synthesized Ce(III) complex. The graph shows the density of states (DOS) spectra for the alpha and beta spin components separately, with the total DOS spectrum scaled by 0.5 and represented by a red line. The chosen energy range was from −25 eV to +10 eV, and the energy level was aligned with respect to the SOMO level (here, SOMO — singly occupied molecular orbital, LUMO — lowest unoccupied molecular orbital). Additionally, SOMO and LUMO images were integrated into

TABLE II

Calculated thermodynamic properties of Ce(III) complex.

Parameter	Value
zero point energy (ZPE)	1278.565 kJ/mol (305.584 kcal/mol)
thermal correction to internal energy (U)	1372.101 kJ/mol (327.940 kcal/mol)
thermal correction to enthalpy (H)	1374.579 kJ/mol (328.532 kcal/mol)
thermal correction to Gibbs free energy (G)	1120.311 kJ/mol (267.761 kcal/mol)
total heat capacity at constant volume (C_V)	619.112 J/(mol K) (147.971 cal/(mol K)
total heat capacity at constant pressure (C_P)	627.427 J/(mol K) (149.959 cal/(mol K))
entropy (S)	852.821 J/(mol K) (203.829 cal/(mol K))
$-TS$ (at 298.15 K)	−60.772 kcal/mol
electronic energy E	−6435.6781690 a.u.
E + ZPE ($U/H/G$ at 0 K)	−6435.1911894 a.u.
E + thermal correction to U	−6435.1555636 a.u.
E + thermal correction to H	−6435.1546194 a.u.
E + thermal correction to G	−6435.2514652 a.u.

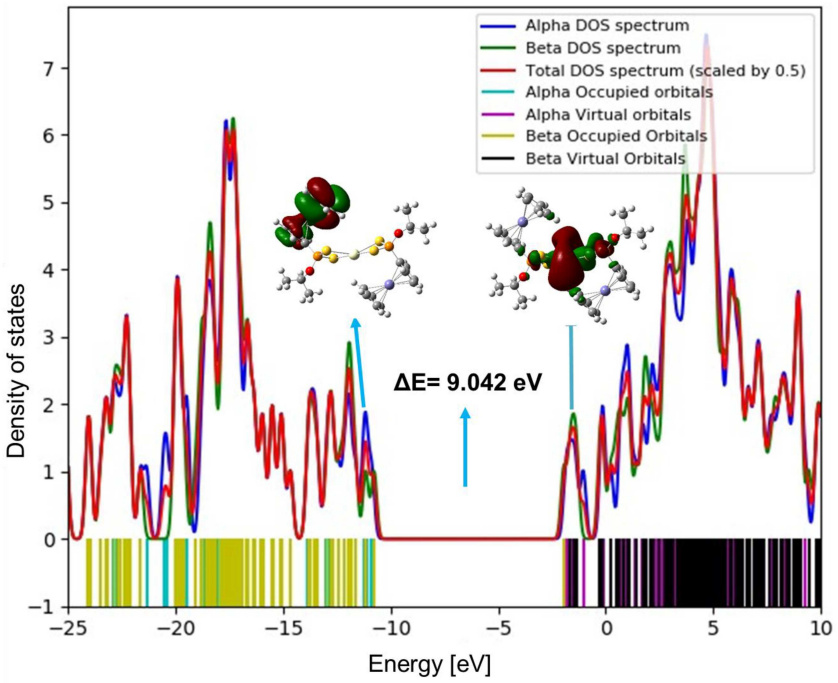

Fig. 7. TDOS graph of Ce(III) complex.

the graph to show the localization of these orbitals on the Ce(III) complex in 3D dimensions. The SOMOs of the Ce(III) complex were located on a ferrocenyl ring of the molecule, while the LUMOs were more clustered around the Ce(III) ion. Therefore, it was determined that the electron transitions were largely due to ligand–metal interactions, and the Ce(III) complex may exhibit potential photophysical or catalytic properties.

An energy band gap (ΔE) of 9.042 eV between the SOMO and LUMO levels was calculated. This wide band gap indicates high electronic stability and low chemical reactivity of the Ce(III) complex [22].

3.2.4. Thermodynamic properties

Some of the calculated thermodynamic parameters of the Ce(III) complex are given in Table II. The calculated data provide detailed information about the structural stability of the molecule and its potential chemical reactivity. Firstly, the electronic energy of the system was determined to be 6435.678 a.u., which is a very low value. This low energy level indicates that the complex is highly stable and can resist reactions requiring high energy barriers. The zero-point energy (ZPE) was calculated to be 1278.565 kJ/mol (305.584 kcal/mol).

This value revealed that the molecule has significant energy, even at the fundamental vibrational energy level, and that this energy contributes to molecular stability.

The calculated internal energy (U), enthalpy (H), and Gibbs free energy (G) with thermal corrections were 1372.101, 1374.579, and 1120.311 kJ/mol, respectively. The difference observed between these values emphasized the importance of the entropic component of the system. In particular, the difference between the free energy correction and the enthalpy clearly revealed the contribution of entropic effects to the thermodynamic equilibrium of the Ce(III) complex. The entropy value was $S = 852.821$ J/(mol K). This high value represents the microstate variability and thermodynamic freedom of the molecule.

In this context, $-TS$ denotes the entropic contribution to the Gibbs free energy, where T is the absolute temperature and S is the entropy of the system. The term $-TS$ accounts for the influence of molecular disorder and thermal motion on the stability of the Ce(III) complex. The value of $-TS$ was determined to be -60.772 kcal/mol, revealing the pronounced effect of the entropic contribution on the free energy. This means that the increase in entropy decreased the free energy of the Ce(III) complex, making the progression of reactions thermodynamically more probable. On the other hand, the heat capacity values of $C_V = 619.112$ J/(mol K) and $C_P = 627.427$ J/(mol K) indicate the capacity of the system to absorb heat. The fact that C_P is higher than C_V reveales that the absorbed heat will be different when the volume and pressure are constant, and the system may show different responses to energy levels that change with temperature. These thermodynamic parameters collectively indicate that the cerium complex has a stable structure supported by high entropy and zero-point energy. Moreover, the thermodynamic data revealed that the Ce(III) complex is not only stable but also capable of maintaining its reactivity over certain temperature ranges.

3.2.5. Nonlinear optical properties

Nonlinear optical (NLO) materials are of great importance for meeting the growing photonic requirements in modern technologies. In this context, complexes containing rare earth elements have remarkable NLO potential due to their large coordination geometries and high electron densities. The nonlinear optical parameters of the synthesized Ce(III) complex were determined by density functional theory (DFT)-based calculations. The nonlinear optical parameters of the Ce(III) complex were calculated at the DFT/B3LYP level of theory using def2-SVP basis sets for the Fe(II) and Ce(III) ions and a 6-311G(d,p) basis set for other atoms. The formulae for the dipole moment (μ), mean polarizability ($\tilde{\mu}$), polarizability anisotropy ($\Delta\alpha$), first hyperpolarizability (β_{tot}), and vector hyperpolarizability (β_{vec}) are as follows

$$\mu = \mu_x^2 + \mu_y^2 + \mu_z^2, \tag{1}$$

$$\tilde{\alpha} = \frac{1}{3}\left(\alpha_{xx} + \alpha_{yy} + \alpha_{zz}\right), \tag{2}$$

$$\Delta\alpha = \frac{1}{\sqrt{2}}\Big[(\alpha_{xx}-\alpha_{yy})^2 + (\alpha_{yy}-\alpha_{zz})^2 + (\alpha_{zz}-\alpha_{xx})^2 + 6\alpha_{xz}^2 + 6\alpha_{xy}^2 + 6\alpha_{yz}^2\Big]^{\frac{1}{2}}, \tag{3}$$

$$\begin{aligned}\beta_x &= \beta_{xxx} + \beta_{xyy} + \beta_{xzz},\\ \beta_z &= \beta_{zzz} + \beta_{xxz} + \beta_{yyz},\\ \beta_y &= \beta_{yyy} + \beta_{xxy} + \beta_{yzz},\end{aligned} \tag{4}$$

$$\beta_{tot} = \sqrt{\beta_x^2 + \beta_y^2 + \beta_z^2}. \tag{5}$$

In addition to β_{tot}, the vector component of the first hyperpolarizability (β_{vec}) — which is experimentally accessible via the EFISH (electric field-induced second harmonic generation) technique — was also calculated. This value reflects the projection of the hyperpolarizability vector along the dipole moment vector and is computed using the expression

$$\beta_{vec} = \frac{|\beta_x\mu_x + \beta_y\mu_y + \beta_z\mu_z|}{\mu}. \tag{6}$$

The values of the parameters obtained using (1)–(6) are given in Table III. The total dipole moment (μ) of the Ce(III) complex was calculated as 1.2461 Debye. This relatively low value indicates that the complex has a symmetric structure and a well-balanced charge distribution.

The mean polarizability ($\tilde{\alpha}$) value of the Ce(III) complex was calculated to be 3299.06 a.u.. This relatively high value indicates that the molecule is highly sensitive to external electric fields and the electron cloud can be easily polarized. Therefore, it was concluded that the ferrocenyl dithiophosphonate ligand, together with Ce(III), delocalizes the electron density more efficiently and thus enhances the optical response. The polarizability anisotropy ($\Delta\alpha$) was found to be 1618.89 a.u. This value, indicative of directionally different electrical behavior, indicates that the Ce(III) complex may be asymmetrically polarizable and show a strong directionally dependent effect on NLO behavior. On the other hand, the first hyperpolarizability (β_{tot}) value of the Ce(III) complex, which also reflects its capacity for second-order nonlinear optical reaction, was obtained as 121.5 a.u.

In addition to the B3LYP method, the CAM-B3LYP functional was employed to accurately describe long-range electron correlation effects and intramolecular charge transfer phenomena. The first hyperpolarizability (β_{tot}) of the Ce(III) complex calculated using CAM-B3LYP was found to be 147.3 a.u., which is significantly higher

TABLE III

NLO properties of Ce(III) complex.

Property	Value		Unit
	B3LYP	CAM-B3LYP	
dipole moment (μ)	1.2461	1.3247	Debye
mean polarizability ($\tilde{\alpha}$)	3299.06	3360.27	a.u.
polarizability anisotropy ($\Delta\alpha$)	1618.89	1652.41	a.u.
first hyperpolarizability (β_{tot})	121.5	147.3	a.u.
vector hyperpolarizability (β_{vec})	92.1	115.6	a.u.

than the B3LYP result (121.5 a.u.). This increase indicates that the nonlinear optical response of the Ce(III) complex benefits from long-range electron delocalization between the ferrocenyl dithiophosphonate ligand and the Ce(III) center. It is worth noting that the B3LYP-calculated β_{tot} value (121.5 a.u.) is approximately eight times higher than that of urea ($\approx$ 15.05 a.u.), a commonly used NLO reference standard [23]. Moreover, the CAM-B3LYP-calculated β_{tot} value (147.3 a.u.) corresponds to nearly a tenfold enhancement relative to urea, further supporting the excellent second-order NLO performance of the Ce(III) complex. These comparative values highlight the molecule's strong polarizability and electron delocalization capabilities. In addition, the mean polarizability ($\tilde{\alpha}$) and polarizability anisotropy ($\Delta\alpha$) values showed slight increases under CAM-B3LYP, confirming the robustness and sensitivity of the complex under long-range corrected DFT analysis. The calculated β_{vec} values were 92.1 a.u. at the B3LYP level and 115.6 a.u. at the CAM-B3LYP level. These results confirm that the Ce(III) complex exhibits a strong second-order nonlinear optical response not only in theory but also in terms of experimental relevance. These findings emphasize the significance of using appropriate functionals for NLO predictions and underline the potential of the synthesized Ce(III) complex in future optoelectronic and photonic material applications.

4. Conclusions

In summary, a novel Ce(III) complex incorporating a ferrocenyl dithiophosphonate ligand was successfully synthesized and thoroughly characterized using a combination of experimental and computational techniques. Spectroscopic analyses confirmed the coordination of the Ce(III) ion via soft sulfur donor atoms, while thermal analysis corroborated the proposed structural formula with the presence of crystallization water. Quantum chemical calculations performed at the DFT/B3LYP level of theory provided valuable insights into the electronic, geometric, and thermodynamic properties of the complex. The significant SOMO–LUMO gap (9.042 eV) revealed exceptional electronic stability, while the MEP and TDOS analyses emphasized the balanced charge distribution and potential ligand-to-metal charge transfer characteristics. Furthermore, the calculated thermodynamic and nonlinear optical parameters highlighted the Ce(III) complex's structural robustness and promising optoelectronic features. These findings not only deepen the understanding of Ce(III) coordination chemistry with ferrocenyl dithiophosphonate ligands but also underscore the potential applicability of such complexes in materials science, particularly in photophysical and nonlinear optical applications.

References

[1] M.K. Rauf, R. Gul, Z. Rashid, A. Badshah, M.N. Tahir, M. Shahid, A. Khan, *Spectrochim. Acta A Mol. Biomol. Spectrosc.* **136**, 1099 (2015).

[2] D.K. Jangid, S.G. Dastider, S. Mandal, P. Kumar, P. Kumari, K.K. Haldar, K. Mondal, R.S. Dhayal, *Chem. Eur. J.* **30**, e202402900 (2024).

[3] I.P. Gray, H.L. Milton, A.M. Slawin, J.D. Woollins, *Dalton Trans.* **17**, 3450 (2003).

[4] M.R.S.J. Foreman, A.M.Z. Slawin, J.D. Woollins, *J. Chem. Soc. Dalton Trans.* **1996**, 3653 (1996).

[5] I. Haiduc, L.Y. Goh, *Coord. Chem. Rev.* **224**, 151 (2002).

[6] E.G. Sağlam, Ö. Çelik, H. Yılmaz, S. Ide, *Trans. Met. Chem.* **35**, 399 (2010).

[7] T.J. Ajayi, M. Ollengo, L. le Roux, M.N. Pillay, R.J. Staples, S.M. Biros, K. Wenderich, B. Mei, W.E. Van Zyl, *ChemistrySelect* **4**, 7416 (2019).

[8] W.E. Van Zyl, J.P. Fackler, *Phosphorus Sulfur Silicon Relat. Elem.* **167**, 117 (2000).

[9] W.E. Van Zyl, J.D. Woollins, *Coord. Chem. Rev.* **257**, 718 (2013).

[10] A. Aydin, N. Acar, H. Yilmaz, *Suleyman Demirel Univ. J. Sci.* **3**, 205 (2008).

[11] P. Çekirdek, A.O. Solak, M. Karakuş, A. Aydın, H. Yılmaz, *Electroanalysis* **18**, 2314 (2006).

[12] M.J. Frisch, G.W. Trucks, H.B. Schlegel et al., Gaussian 09, Rev. E.01 (now Gaussian 16), Gaussian Inc., Wallingford (CT) 2016.

[13] R. Dennington, T.A. Keith, J.M. Millam, GaussView, Rev. 5.0.9 (now GaussView 6), Semichem Inc., Shawnee Mission (KS) 2009.

[14] A.D. Becke, *J. Chem. Phys.* **98**, 5648 (1993).

[15] C. Lee, W. Yang, R.G. Parr, *Phys. Rev. B* **37**, 785 (1988).

[16] F. Weigend, R. Ahlrichs, *Phys. Chem. Chem. Phys.* **7**, 3297 (2005).

[17] N.M. O'Boyle, A.L. Tenderholt, K.M. Langner, *J. Comput. Chem.* **29**, 839 (2008).

[18] T. Lu, Q. Chen, *Comput. Theor. Chem.* **1200**, 113249 (2021).

[19] P.M. Das, W. Kuchen, H. Keck, G. Haegele, *J. Inorg. Nucl. Chem.* **39**, 833 (1977).

[20] J. Petrova, S. Momchilova, E.T. Haupt, J. Kopf, G. Eggers, *Phosphorus Sulfur Silicon Relat. Elem.* **177**, 1337 (2002).

[21] A.A. Pinkerton, D. Schwarzenbach, *J. Chem. Soc. Dalton Trans.* **23**, 2466 (1976).

[22] K. Fukui, *Science* **218**, 747 (1982).

[23] C. Adant, M. Dupuis, J. L. Bredas, *Int. J. Quant. Chem.* **56**, 497 (1995).